BULLETIN OF THE POLISH ACADEMY OF SCIENCES
TECHNICAL SCIENCES, Vol. 72(6), 2024, Article number: e151674
DOI: 10.24425/bpasts.2024.151674

Experimental and numerical static tests of tensegrity triplex modules

Andrzej RUTKIEWICZ* **and Leszek MAŁYSZKO**

Faculty of Geoengineering, University of Warmia and Mazury in Olsztyn, Poland

Abstract. The paper presents chosen results of experimental tests performed on physical mock-ups of tensegrity triplex modules, approximately 1.2 m tall and of 0.5 m diameter, made of steel. A uniform and uniaxial static compressive loading is applied to three upper nodes of the modules at six different self-stress levels. Cable forces are measured using specially crafted force transducers of an electro-resistive strain-gauge type. Two types of struts with different slenderness are incorporated to analyze the influence of buckling on the behaviour of the modules. A simple three-parameter mathematical model is presented to explain the behaviour of the modules and discuss the obtained experimental data. The results show nonlinear behaviour in the equilibrium path, as well as, rapidly decreasing axial stiffness in the post-critical phase. An increase in prestress has a small influence on the stiffness in the chosen range of compressive loading. The experimental results are valuable for purposes of verification and validation of numerical studies and fill the lack of experimental data in the literature.

Keywords: experimental test; tensegrity triplex; self-stress level; force transducers; struts buckling.

1. INTRODUCTION

Tensegrities are regarded as a unique class of spatial trusses where members are connected in a self-equilibrated system providing stability and geometrical stiffness to the whole system. Their analysis starts with finding the infinitesimal mechanisms and self-stress states, which influence their static and dynamic responses to external loading. More basic information on tensegrities can be found in [1–3]. As practice shows, there are many mistakes regarding considering whether the structure is a tensegrity or not – the matter was taken care of in [4]. Moreover, the statics of these structures are unique and sophisticated, for basic information please refer to [5].

Research in tensegrities is currently performed in many fields of science, mainly including robotics [6], aerospace [7–9], deployable [10,11], offshore [12], and civil engineering. In the last field, studies are focused on structures such as – domes [13–16], footbridges [17,18], solar panels [19], tents [20], facades [21], and drilling rigs [22] to mention just a few. In general, it can be concluded that all of these multidisciplinary fields draw from tensegrity intrinsic and unique mechanical features.

Here, we are focusing on static response to a compressed tensegrity triplex module, which can be used in the future as a civil engineering column or as part of the support of other structures. Regarding column-like tensegrity elements, the triplex was analyzed in a few experimental and some numerical studies connected with its static behaviour and stability. Triplex was previously analyzed under compressive loading in [23–27], where an analytical mathematical model based on force equations of equilibrium was presented and, in most cases, solved numerically. Struts were defined as perfectly straight bars with no initial imperfections. This approach can be of use in civil engineering structures, where buckling of elements is forbidden. The design of such modules was preliminarily analyzed in [28]. In [29–31] tensegrity modules were calculated using struts modelled as bars with initial curvature imperfection, which causes them to behave as a beam. In such a case, an increase in loading applied on strut results in the growth of the lateral deflection of the middle section, which is called a second order effect. These models were utilized in the field of biotechnology for describing cell behaviour or in aerospace engineering for analyzing planetary landers. Biology-based analyses can often be conducted as quasi static. In planetary landers buckled struts are able to store large amounts of elastic energy, which is accumulated and released during landing impacts.

All of these analyses are mainly numerical and not many experimental tests were conducted up to date. An exception in similar scale is a recent work [32], where some static tests were performed. However, it was recognized that the prestress level, the local bucking behaviour of struts and rupture characteristic of cable elements have a dominant effect on the collapse of the whole system. The objective of the experimental tests reported here was to evaluate the accuracy of the numerical procedure and to analyse the influence of the prestress level on the behaviour of the tensegrity column working under a static load. The experimental tests focused on the static axial response, considering six different prestress levels and two different types of struts.

2. MATERIALS AND METHODS

2.1. Physical mock-ups of tensegrity modules

The tensegrity triplex contains six nodes denoted as n_i lying in two parallel planes. It is built from six base cables with lengths denoted as l, three cross cables with lengths denoted as s, and

*e-mail: andrzej.rutkiewicz@uwm.edu.pl

Manuscript submitted 2024-05-22, revised 2024-07-24, initially accepted for publication 2024-08-08, published in November 2024.

three struts with lengths denoted as b. The module height is denoted as h and base cables create two bases, in which a circle of radius r can be described. If needed, the schematics of nodes and elements are presented in Fig. 4a for a better understanding of the system.

Here, two types of tensegrity triplex physical mock-ups were tested – i.e. ones with *slender* and *stocky* struts. *Slender* struts were made of *M20* bars (Fig. 1a), while *stocky* struts were made of 42.4 × 2.0 mm circular hollow sections, in which *M20* bars were welded into their edge parts (Fig. 1b). Both struts were made of *S355* steel and had almost the same cross-sectional area, although different second moment of inertia. Besides this difference, the geometry and cross sections of both modules remained the same – see Table 1 for details.

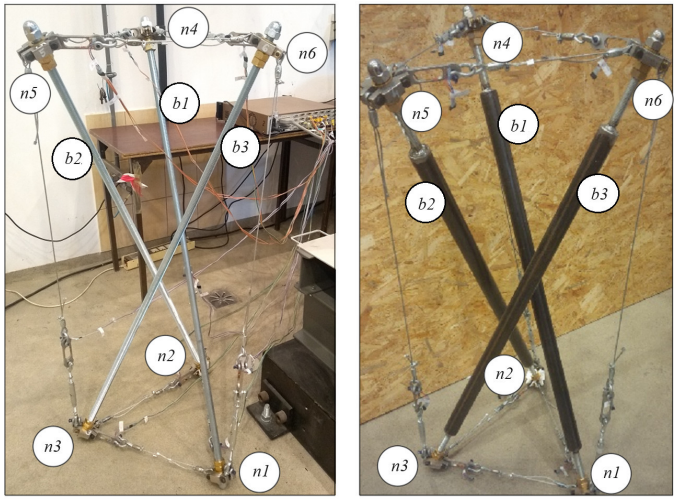

(a) (b)

Fig. 1. Triplex mock-ups with (a) slender struts and (b) stocky struts

Table 1
Geometry of the physical triplex mock-ups

Lengths (m)							
Height h		Strut b		Cross cable s		Base cable l	Radius r
1.186		1.280		1.193		0.431	0.249
Coordinates X Y Z (m)							
n_1	0.249	0	0	n_4	–0.216	0.125	1.186
n_2	–0.125	0.216	0	n_5	0	–0.249	1.186
n_3	–0.125	–0.216	0	n_6	0.216	0.125	1.186

The cross and base cables were created using a 3 mm nominal diameter steel line made of 19 wires and thimble on each side with a cross-sectional area of 5.25 mm^2. The cross cables had also built-in Roman screws to perform the prestressing. The nodes were laser cut out of a 20 mm thick stainless-steel sheet and further countersigned for *M8* bolts, which held the cables. A connection of the bars and nodes was created by a regulation of two steel nuts, while the connection of cables and nodes was created using *M8* screws.

2.2. Methodology and the equipment

The testing program was divided into two parts: 1) tests on *slender* and *stocky* struts, as well as 2) tests on physical mock-ups of *slender* and *stocky* triplex modules.

Before describing the tests, a comment on some material properties needs to be made. Previously to the described here tests, uniaxial tension tests of cross and base cables were performed to determine experimentally the equivalent Youngs' moduli. This was important since the cables are composites built from steel lines and force transducers, as well as in the case of cross cables, Roman screws – see Fig. 1. The equivalent moduli of the cross and base cables were 81 and 56 GPa, respectively. Moreover, Young's module was also determined for the *M20* bars in tension tests. The theory of elasticity does not distinguish the values of Young's module in tension and compression; therefore it was acceptable from the theoretical point of view. Since the *stocky* strut is composed of a circular hollow section, its moduli were assumed the same as the *M20* bar but recalculated due to the slight difference in cross-sectional area. The obtained Youngs' moduli were 204.1 and 197.8 GPa for the *slender* and *stocky* struts, respectively.

A total of six tests for struts were performed – three for the *stocky* and three for the *slender* ones. The material and cross-section properties of struts are presented in Table 2, where m is the unit mass, f_y is the yield strength, A is the cross-section area, l_0 is the initial length, I_b is the second moment of inertia, i is the radius of gyration, λ is the slenderness and d is the threaded diameter of M20 bar.

Table 2
Material and cross-section properties of struts

Material		
Element	m (kg/mb)	f_y (MPa)
Slender struts (*M20*)	1.92$^{(1)}$	355$^{(1)}$
Stocky struts (*RO42,4x2*)	1.99$^{(2)}$	355$^{(1)}$

Cross-sectional characteristics					
Element	$A^{(1)}$ (mm^2)	l_0 (mm)	I_b (mm^4)	i (mm)	λ (–)
Slender struts	225.2	1370	4036$^{(3)}$	4.23	323.9
Stocky struts	253.8	1370	51 916	14.3	93.7

$^{(1)}$ Manufacturer. $^{(2)}$ Weighted. $^{(3)}$ $I = \pi d^4/64$ for d = 16.933 mm.

The testing standpoint is presented in Fig. 2a, where struts were connected to supports through the ball joint system. For the *stocky* struts only the compressive force S and vertical displacement u were measured, whereas for the *slender* struts also the increase in lateral deflection of the middle section w_m was measured (Fig. 2). The tests were carried out in the laboratory of the Department of Mechanics and Building Structures of the University of Warmia and Mazury in Olsztyn using a universal testing machine with a nominal force of 300 kN and class 0.5 [33] with BlueHill software [34]. The machine gave

information on force S and vertical displacement u. The lateral deflection of the middle section w_m was measured using two displacement sensors. For testing the modules, an adaptation of the base and loading plate of the machine was designed using Autodesk Inventor [35]. The new base makes it possible to test the regularly used bottom handle of the machine without dismantling and is made of two IPN 220 I-beams with a length of 0.76 m, four IPN 140 I-beams with a length of 0.71 m and a steel sheet with a thickness of 4 mm (see Fig. 3a, where the steel sheet is removed). The main component of the new loading plate is a thrust bearing that allows rotation around the loading axis, with a high compressive load capacity of 335 kN (Fig. 3b, in the upper part is the metal case for the bearing is shown, which is painted in white in the bottom part of the figure). Crafted specially for the models, the force sensors were attached to all nine cables and were designed to work with electro-resistive strain gauges as a *Wheatstone half-bridge*, where two active arms are placed on the opposite sides of the four-arm bridge. The body of the sensor was precisely water-cut out of a 6 mm thick stainless-steel sheet and further processed to obtain a clear surface. The strain gauges were mounted on the two inner sides of the body, with special attention to manufacturers' requirements. The force sensors were also calibrated for the force using the strain-gauge bridge and a testing machine obtaining a force-strain function and for the temperature using the strain-gauge bridge and climate chamber obtaining a temperature-strain function. The testing standpoint is presented in Fig. 4b.

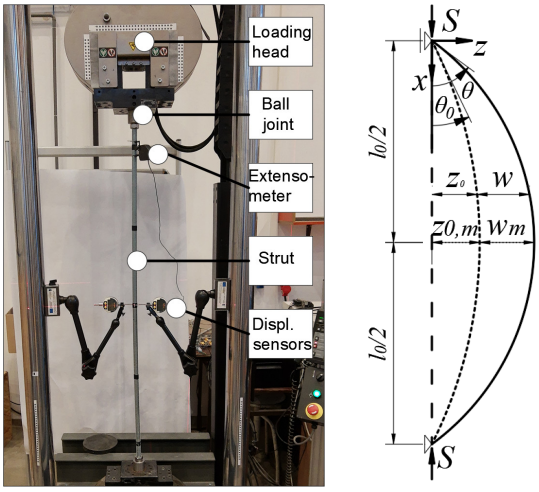

(a) (b)

Fig. 2. Strut tests: (a) standpoint view and (b) schematics of strut with initial imperfection and lateral deflection

The tensegrity modules under consideration are characterized by the one self-stress state that is introduced initially in the members before applying external loads. The levels of the self-stress state can be defined as the normal elongation of the cross cables, i.e. the strain $p_0 = (s_0 - s_n)/s_n$, where s_n is the natural (unstressed) length of the cross cable and s_0 is the length of the cross cable after prestressing the module. All lengths and forces are theoretically the same in each cross cable if symmetrical configurations of the self-stress state are assumed. After pre-

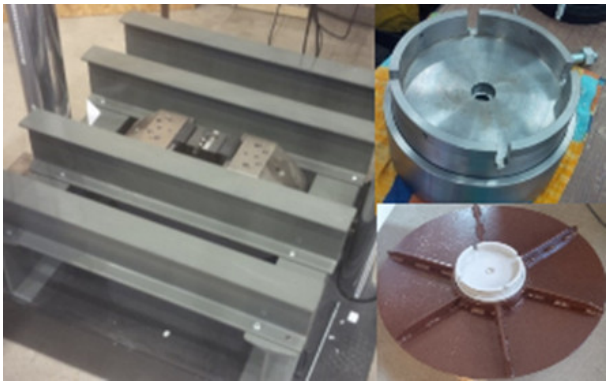

(a) (b)

Fig. 3. Adaptation of (a) base and (b) loading plate

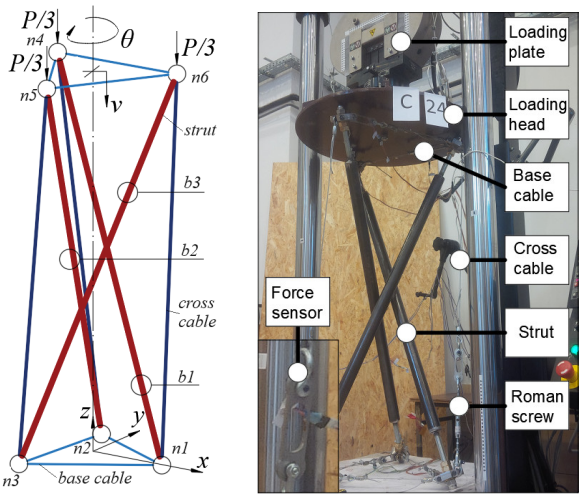

(a) (b)

Fig. 4. Module test: (a) schematics and (b) standpoint view

stressing, the length of the cross cable is equal to $s_0 = s_n(1+p_0)$, while the force is equal to $N_{s0} = E_s A_s p_0$, where $E_s A_s / s_n$ is the elastic axial stiffness. The lengths and forces in base cables and struts can be theoretically calculated based on the self-stress states and the lengths of elements. The tests on the tensegrity modules were performed at six prestress levels for each of the two types of struts. The levels of the self-stress state applied in the experimental tests are shown in Table 3 as the normal pre-strain of the cross cables, together with the values of the prestressing forces. Please note that the theoretically calculated forces in base cables are different than forces measured in the physical mock-ups.

The prestressing procedure was as follows. At the beginning of each prestress level, the module was dismounted to set the forces in the transducers to zero. Afterwards, the module was reconnected, and the roman screws were adjusted to activate the geometrical stiffness and introduce the proper prestress level. Next, the external load was applied using the loading plate, which was mounted on a ball joint and enabled to freely rotate along the vertical loading axis z. Each prestress level contained approximately 25 loading steps with intervals of approximately

Table 3
Self-stress levels (mean values for both modules)

Self-stress levels	1	2	3	4	5	6
p_0 ($\mu\varepsilon$)	700	1675	2732	3778	4940	5945
cross cables (N)[1]	298	712	1165	1608	2102	2532
base cables (N)[1]	65	177	300	407	1055	630
base cables (N)[2]	62	150	245	338	440	532
struts (N)[2]	–320	–768	–1252	–1732	–2268	–2732
[1] Measured, [2] Calculated						

300 N. The loading plate mass induced the initial loading compressive force P_0 equal to 1 kN. The testing devices used during the tests were: the testing machine with the loading plate, which gave information on the external load P and vertical displacement v, the strain gauge bridge, which gave information on the forces in the cross cables N_s and the base cables N_l, and the grid glued on the loading plate rotational part, which gave information on angle of rotation between the upper base of the triplex and the lower base of it, signified as θ. Please note that the vertical displacement in the local system of the strut is denoted as u, while the global vertical displacement of the module is denoted as v. Similarly, the local force compressing a single strut is denoted S, while the global force compressing the module is denoted P.

2.3. The three-parameter model for tensegrity

In Fig. 5 a *three-parameter model* of behaviour for the compressed tensegrity triplex is presented. Two kinematic parameters are the angle between the strut chord and the horizontal direction α and the axial displacement of the strut chord u, while the static parameter is the prestressing force in the strut N_b^0. The model assumes, that the strut is axially inextensible, which means that the length of the strut remains constant and is equal to s. However, it considers the bending stiffness EI_b. In the initial configuration, the strut chord length is equal to l_0, imperfection to $z_{0,m}$, total length to s and its chord is inclined to the horizontal direction at an angle α_0. No forces are applied to the system and the elastic support does not induce any force.

Next, the prestressing force in the strut N_b^0, as well as, the external force equal to $P/3$ induces the actual configuration in which the angle α_0 changes to α, as well as the chord of the strut displaces at value u. The spring support reaction R is equal to the product of its stiffness k_l and displacement t. The stiffness k_l is calculated based on the stiffnesses of two base cables of the tensegrity triplex, which are tensioned during compression and are equal to:

$$k_l = \sqrt{3}\, E_l A_l / l_l\,, \tag{1}$$

where E_l, A_l and l_l are the Youngs modulus, cross-sectional area, and natural length of base cables, respectively. The displacement t is equal to (Fig. 5)

$$t = l_0 \cos(\alpha_0) - \left(l_0 - u\right)\cos(\alpha). \tag{2}$$

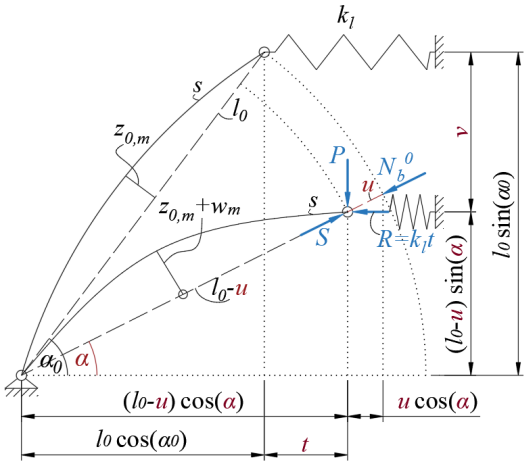

Fig. 5. A three-parameter model for tensegrity

The relation between the lateral displacement of the middle section w_m and the axial displacement of the chord u is

$$w_m = -z_{0,m} + 0.5\sqrt{4z_{0,m}^2 - u^2 + 2l_0 u}\,. \tag{3}$$

The global vertical displacement v is calculated as (Fig. 5)

$$v = l_0 \sin(\alpha_0) - \left(l_0 - u\right)\sin(\alpha). \tag{4}$$

Since there are two parameters, only two static equations of equilibrium are needed. The proposed equations are (Fig. 5):

$$\begin{aligned} P\left(l_0 - u\right)\cos(\alpha) - 3R\left(l_0 - u\right)\sin(\alpha) &= 0, \\ S - R\cos(\alpha) - (P/3)\sin(\alpha) - N_b^0 &= 0. \end{aligned} \tag{5}$$

The relation between the force in the strut S and the lateral deflection of the middle section w_m is applied as in equation (7), which is further explained below.

A nonlinear system of equations (5) has two unknown values α and u. The prestressing force N_b^0 is constant and chosen at the prestressing phase. External load P is substituted by summing the incremental values of ΔP. To draw the equilibrium paths, the system (5) is solved multiple times for an increasing value of P in each iteration. Here, we use the Matlab [38] *fsolve* function, which numerically finds the solution.

The presented model demonstrates only the behaviour of the strut in its plane. The module also rotates along the vertical, central axis z, which generates additional and main vertical displacements due to rigid body movements of struts. These movements are connected with the infinitesimal mechanisms and can achieve significant values even thou the loading may be relatively small. The purpose of the presented *three-parameter model* is to present a discussion in the next section.

3. RESULTS

3.1. Experimental results

First, the results of the strut tests are presented. In the buckling tests, the *slender* struts were treated as elastic pin-ended columns

with the bending stiffness EI_b, for which the Eurocode buckling curves can be applied [36]. The curve c was chosen for the reduction factor of the strut resistance as a function of its generalized slenderness $\overline{\lambda} = \lambda/\lambda_1 = 4.24$ (where $\lambda_1 = \pi\sqrt{E/f_y} = 76.41$). This value of the slenderness is expected to predict a fully elastic buckling. The generalized slenderness of the *stocky* struts is $\overline{\lambda} = 1.23$, which means the elastoplastic bucking. The displacements of the *slender* strut were dominated by changes in curvature facilitating the consideration of the elastic beam to be inextensible with initial imperfections $z_0(x)$. To determine the Euler critical load P_E of the *slender* strut based on the experimental test, the lateral deflection of the middle section w_m was measured at various values of the external load S. Utilizing the well-known equation from specifications of structural engineering code in the form $z(x) = z_0 + w = z_0/[1-(S/P_E)]$, we can obtain the *Southwell plot* with a straight regression line

$$w_m = P_E w_m/S - z_{0,m}\,, \tag{6}$$

which yields the critical load and the initial imperfections $z_{0,m}$ in the middle by using the approximation method of least squares (Fig. 6). More information on the plot can be found in [37]. Three *slender* struts were tested giving the following results: for *b1* strut $P_E = 4174$ N and $z_{0,m} = 5.05$ mm, for *b2* strut $P_E = 4027$ N and $z_{0,m} = 3.44$ mm and for *b3* strut $P_E = 4497$ N and $z_{0,m} = 7.98$ mm. The blue line shown in Fig. 6 is the imperfection proposed by the Eurocode for the initial imperfection $z_{0,m} = l_0/200 = 6.85$ mm, and the theoretical value of Euler load $P_E = 4332$ kN.

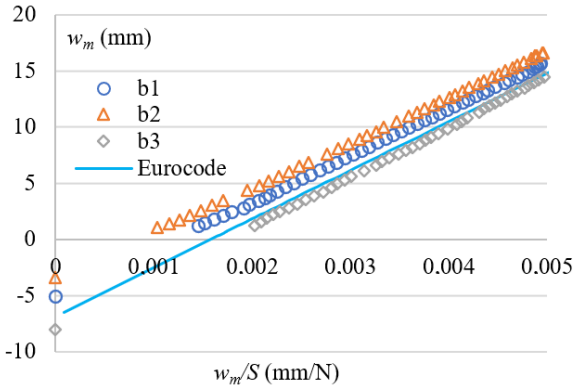

Fig. 6. The Southwell plot for slender struts

Experimental results also fit into the relation for relative coordinates presented in [37]:

$$\frac{S}{P_E} = \frac{w_m}{w_m + z_{0,m}}\left[1 + \frac{\pi^2}{8}\left(\frac{w_m}{l_0} + \frac{z_{0,m}}{l_0}\right)^2\right], \tag{7}$$

and presented in Fig. 7. As can be seen, the fit accuracy is perfect. This equation is obtained by the approach of an equilibrium analysis and is applicable if inevitable imperfections must be considered, regardless of their initial shape and type. Note that the theoretical prediction of the critical load $P_E = EI\pi^2/L^2 = 4.33$ kN is greater than the experimental value by 8%. Considering that the expression (7) is based on the linearized small-deflection theory and that only three struts were tested, this difference should be considered quite satisfactory. Comparing the data points in the lower left and upper right corner of the plot, we can see that the deviation from the straight regression line in the lower left corner is greater than in the right. However, if we discard the results from a few initial load steps as prone to greater errors, the difference between the theoretical and experimental values of the critical load will decrease only by 1%. What is important is that we can conclude that equation (7) is properly describing the behaviour of struts and therefore it is well suited to be used with the *three-parameter model* from Section 2.3.

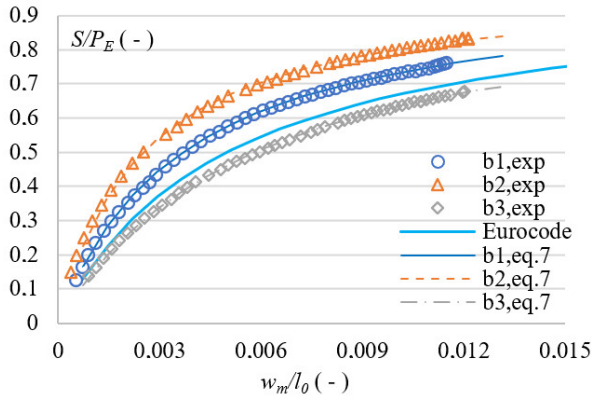

Fig. 7. Relative equilibrium path – experiment and equation (7)

The results presented in the form of force S versus axial displacement u chart of the compression tests performed on the *stocky* struts are shown in Fig. 8. Additionally, for comparison purposes, the results of the *slender* struts were also drawn. As can be seen, the stiffness of the stocky struts is linear, and this information is important when considering the results of the compressed modules.

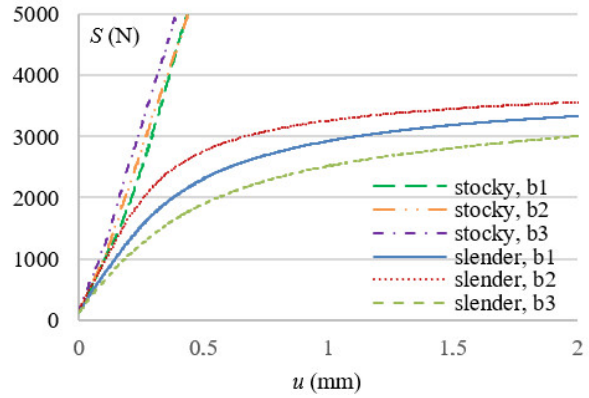

Fig. 8. Equilibrium path for both types of struts

Next, the results of tests performed on physical mock-ups of tensegrity modules are presented. In the upper part of Fig. 9, the equilibrium paths for six tests for two types of mock-ups and three prestress levels are shown (other results were removed due to clarity). As can be seen, the change of the stiffness is nonlinear

in both cases. The stiffness of the *stocky* mock-up increases up to the end of the test, while the stiffness of the *slender* mock-up increases up to the value of approximately 3 kN and vertical displacement of 3 mm, and afterwards a change of curvature flexion appears. The stiffness is still increasing yet at a slower rate. The change in the chart relates to the buckling of *slender* struts analyzed at the beginning of this section. The equilibrium paths can be approximated by 2nd and 3rd polynomials for the *stocky* and *slender* mock-ups, respectively.

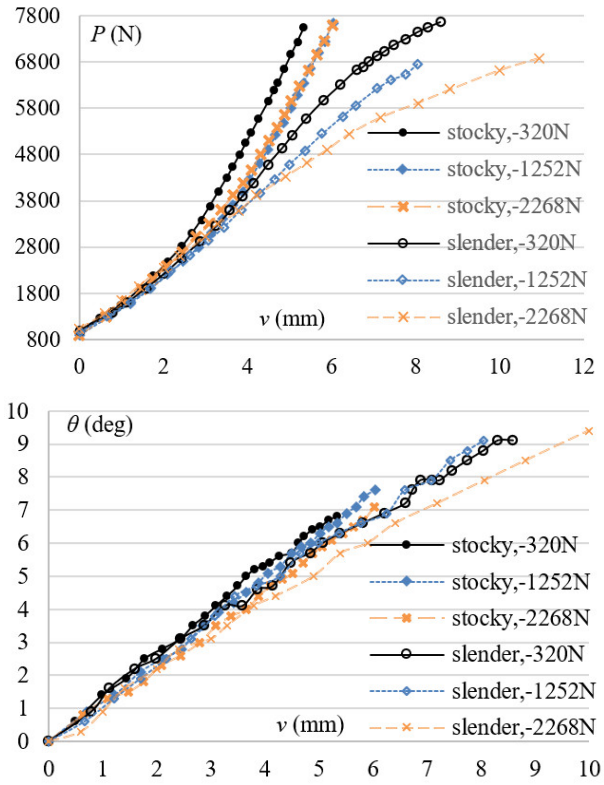

Fig. 9. The equilibrium path for six selected tests

In the lower part of Fig. 9 the relation between the displacement v and the rotation of the upper base θ is shown for the same tests. As can be seen, the relation is linear for both mock-ups, which means that regardless of the strut type, the vertical displacement can be easily correlated with the upper base rotation by a linear function. Both models lose their stiffness in axial compression as the prestress level increases. Comparing the values of displacement v for both mock-ups at the same level of external loading P, the displacement in the *slender* mock-up is approximately 50% higher than in the *stocky* one. We can clearly conclude that the increase in prestressing is counterproductive (or at least has a negligible effect) in terms of stiffness in axial and uniform compression.

The relationship between forces in cross cables and the vertical displacement for both mock-ups is presented in Fig. 10 for all prestress levels. Note, that the member forces are the mean value calculated from the three cross-cable readouts. In the *stocky* mock-up, the stiffness increase is constant, while in the *slender* mock-up, the increase stops at a certain point and afterwards decreases. Moreover, the greater the prestress, the point of equilibrium change occurs earlier in the path. For example, the 6th prestress level curve is decreasing from the beginning of the loading. Also, the magnitude of change of force values in cross cables for higher prestress levels decreases.

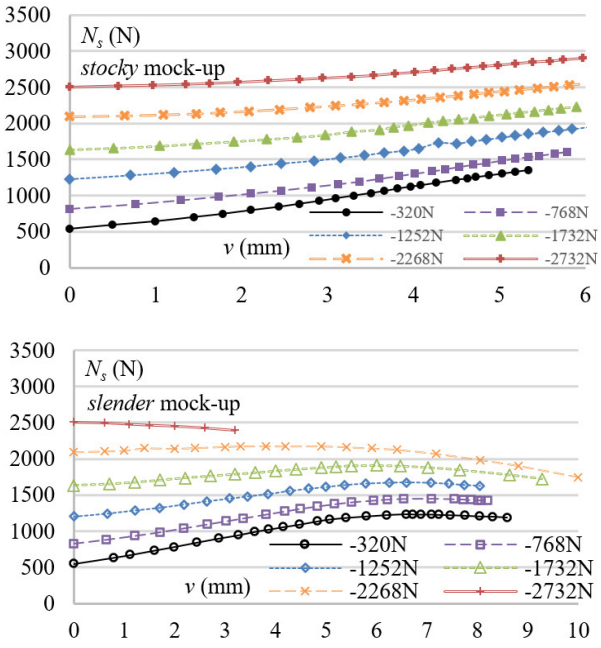

Fig. 10. Forces in cross cables in relation to displacement

Figure 11 presents changes in base cables in relation to displacement. Their behaviour is similar to the behaviour presented by the equilibrium paths. For *stocky* mock-ups, the forces are constantly increasing, while for *slender* mock-ups, they increase to a certain point, at which the magnitude of the increase starts

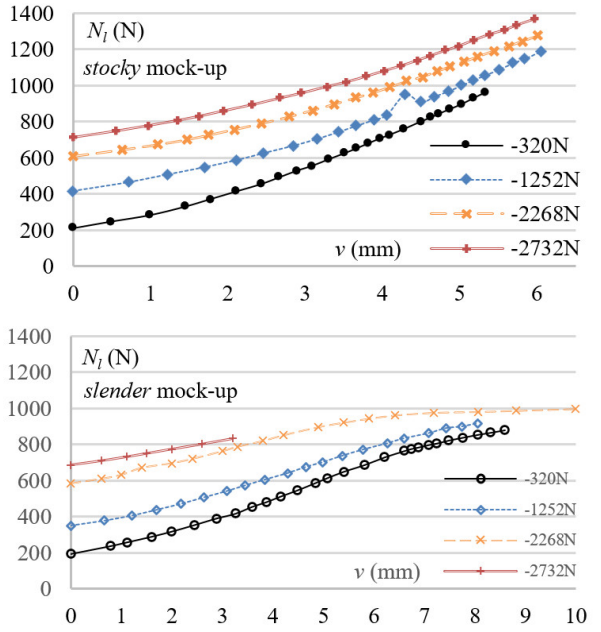

Fig. 11. Forces in base cables in relation to displacement

to be significantly smaller. Again, we can connect this phenomenon with the *slender* struts buckling, i.e. the *slender* struts axial stiffness is low and therefore the mock-ups can more easily displace axially.

3.2. Numerical verification

Here, a mathematical model presented in Subsection 2.3 is compared with the experimental results. Moreover, a comparison with a three-degree-of-freedom spatial model based on the force density method (called here as *FDM* for convenience) from [24] and [26] is shown. The *FDM* model is built based on force equations of equilibrium in the actual configuration; however, it implements struts as perfectly straight with axial stiffness equal to EA/L. Equation (7) on the contrary, as shown in Subsection 3.1, considers strut imperfections and second-order theory. However, it does not include the spatiality of the triplex module. The data implemented in the *FDM* model is given in Table 1 and Table 2, as well as supplementary information given in Subsections 2.1 and 2.2. The *FDM* model was calculated on data as follows: $\alpha_0 = \arcsin(h/b) = \arcsin(1186/1280) = 67.9°$ (Table 1), $z_{0,m} = 6.85$ mm (Eurocode recommendations), $N_b^0 = (2732-320)/2 = 1206$ N, $k_l = \sqrt{3}E_lA_l/l_l = \sqrt{3}\cdot 56\cdot 10^3\cdot 5.25/431 = 1181$ N/mm (base cable stiffness) and $l_0 = 1370$ mm (Table 2). The differences between the *stocky* and *slender* mock-ups are due to the different moments of inertia I_b as presented in Table 2. The experimental results for the *slender* and *stocky* mock-ups and all six prestress levels, as well as two mathematical models are presented in Figs. 12 and 13, respectively. The forces in base cables for the *stocky* mock-ups for six experimental tests and two mathematical models are presented in Fig. 14.

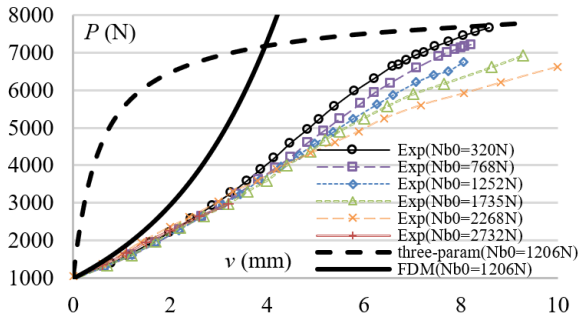

Fig. 12. The slender module numerical and experimental results

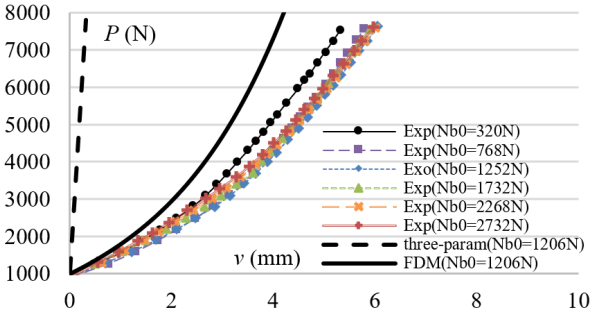

Fig. 13. The stocky module numerical and experimental results

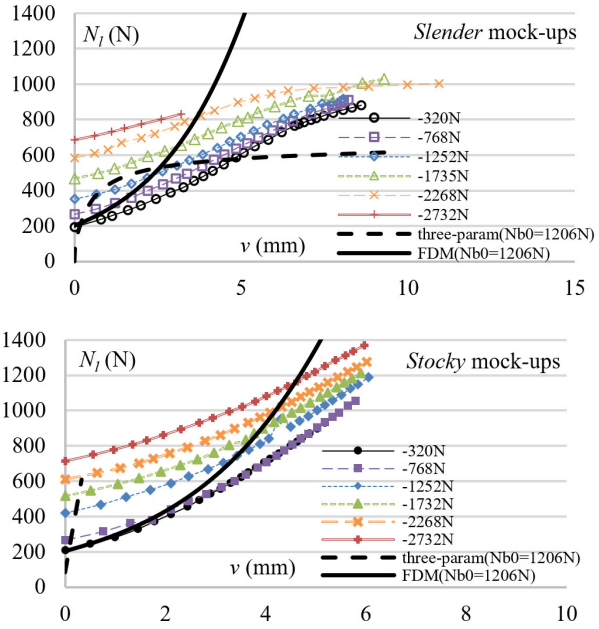

Fig. 14. The stocky and slender module base cable forces

4. DISCUSSION

The *three-parameter model* precisely takes into account the reduced stiffness of struts, as written in equation (7), however it does not fit the results well – see Fig. 12. It presents an overstiffened reaction to the loading. The *FDM* model fits the data quite well only at the beginning of the loading process, since it does not take into account the imperfections of the struts – see again Fig. 12. The triplex module possesses a so-called infinitesimal mechanism, which causes it to significantly rotate (angle θ in Fig. 4a) and compress (displacement v in Fig. 4a) for small values of loading force P. This phenomenon is common for tensegrities. Since the *three-parameter model* does not include the possibility for the triplex to rotate along the θ angle, thus its response is high in comparison to the experimental results. However, we know that it describes precisely the behaviour of the strut itself – see Fig. 7. On the contrary, the *FDM* model accounts for the rotation and the actual node configuration of the triplex and thus takes into account the infinitesimal mechanism phenomenon. Therefore, it is well suited to describe the experimental results for *stocky* mock-ups, as shown in Fig. 13. Small differences are expected to originate from the theoretical and actual material differences due to the high complexity of physical mock-ups. The *three-parameter model*, which does not include the rotation of the upper base, again does not fit the experimental results in Fig. 13. In the case of base cable forces presented in Fig. 14, the *FDM* model relatively well describes the changes of forces in base cables for the *stocky* module and only initially well for the *slender* module. On the contrary equation (7) describes better the forces in base cables in the case of the *slender* module. To better describe the behaviour of the *slender* module, the *FDM* model ought to be supplemented with equation (7) for the description of strut behaviour. Then it is expected to fit the experimental data well.

5. CONCLUSIONS

In the paper results of compressed experimental tests on two physical mock-ups of tensegrity triplex at different pre-stress levels and for different struts were presented. The results are valuable since there is not much experimental data found on the subject in the literature. The advantage of this test, regarding some other tests, is that it also contains information on the prestress levels of the structure and directly measures forces in cables of the tensegrity structure. The results facilitate the verification and validate numerical solutions available in the literature.

Moreover, a simple *three-parameter model* for the description of tensegrity behaviour was presented. The model is moderately accurate with the results; however, it enables for better understanding of the triplex behaviour, especially in comparison to the more precise model from other publications. It takes into account the nonlinear behaviour of the strut, yet it does not include the rotation of the triplex module during compression. For example, it enables to conclude that, in order to build a highly stiff module, it is more beneficial to eliminate the infinitesimal mechanisms, rather than strengthen the struts.

From the point of view of this survey, the mechanical models of tensegrity behaviour can be divided into two parts. First describe struts as perfectly straight bars, with no imperfections, which results in inducing only axial internal forces in them. These models can be verified/validated by the *stocky* module experimental results and can be utilized in the Civil Engineering field. In the field, due to high stiffness requirements, buckling of struts is not allowed and imperfections and second-order effects can be implemented into resistances of elements [36] – this simplified analysis is accurate enough for the task.

The second part describes struts as bars with initial curvature imperfection, which causes them to behave as a beam. Furthermore, an increase in loading results in the growth of the vertical displacement (a second-order effect – see Fig. 2b). Such models are utilized in the field of Biotechnology for describing cell behaviour or in Aerospace Engineering for analyzing planetary landers. Biology-based analyses can often be conducted as quasi-static. In planetary landers buckled struts can store large amounts of elastic energy, which is accumulated during landing ground impacts. For the verification/validation of such theoretical models, the *slender* module experiment is suitable.

Further work includes numerical finite element method analyses, as well as the implementation of equation (7) into the *FDM* model to close the gap between the theoretical calculations and experimental results.

REFERENCES

[1] R. Motro, *Tensegrity. Structural Systems for the Future*, London, GB: Kogan Page Science, 2003.

[2] R.W. Burkhardt, *A practical guide to tensegrity design*, Cambridge, USA, 2004.

[3] R.E. Skelton and M.C. de Oliveira, *Tensegrity systems*, London, GB: Springer, 2009.

[4] P. Obara, J. Kłosowska, and W. Gilewski, "Truth and Myths about 2D Tensegrity Trusses," *Appl. Sci.*, vol. 9, no. 1, p. 10179, 2019, doi: 10.3390/app9010179.

[5] J.M. Mirats Tur and S.H. Juan, "Tensegrity frameworks: Dynamic analysis review and open problems," *Mech. Mach. Theory*, vol. 44, no. 1, pp. 1–18, 2009, doi: 10.1016/j.mechmachtheory.2008.06.008.

[6] Y. Liu, X. Yue, J. Wu, B. Yang, and Y. Li, "A review on tensegrity structures-based robots," *Mech. Mach. Theory*, vol. 168, p. 104571, 2022, doi: 10.1016/j.mechmachtheory.2021.104571.

[7] Sh. Li *et al.*, "Structural design and integral assembly procedure of rigid-flexible tensegrity airship structure," *Eng. Struct.*, vol. 284, p. 115803, 2023, doi: 10.1016/j.engstruct.2023.115803.

[8] Y. Tang, T. Li, Q. Lv, and X. Wang, "A self-vibration-control tensegrity structure for space large-scale construction," *Mech. Syst. Signal Process.*, vol. 177, p. 109241, 2022, doi: 10.1016/j.ymssp.2022.109241.

[9] H. Zou, L. Wu, W. Li, F. Han, and Z. Deng, "Thermally-induced vibration analysis of tensegrity modules during space deployment using dynamic stiffness method," *Int. J. Solids Struct.*, vol. 282, 112454, 2023, doi: 10.1016/j.ijsolstr.2023.112454.

[10] T. Habibi, L. Rhode-Barbarigos, and T. Keller, "Effects of prestress implementation on self-stress state in large-scale tensegrity structure," *Eng. Struct.*, vol. 288, p. 116222, 2023, doi: 10.1016/j.engstruct.2023.116222.

[11] W. Xu, J. Zhang, H. Guo, R. Liu, and Z. Kou, "Design of a deployable aerodynamic decelerator based on a tensegrity structure," *Acta Astronaut.*, vol. 215, pp. 315—324, 2024, doi: 10.1016/j.actaastro.2023.11.047.

[12] I. Hrazmi, J. Avenseng, J. Quirant, and F. Jamin, "Deployable double layer tensegrity grid platforms for sea accessibility," *Eng. Struct.*, vol. 231, p. 111706, 2023, doi: 10.1016/j.engstruct.2020.111706.

[13] Y. Feng, X. Yuan, and A. Samy, "Analysis of new wave-curved tensegrity dome," *Eng. Struct.*, vol. 250, p. 113408, 2022, doi: 10.1016/j.engstruct.2021.113408.

[14] N. Logzit and K. Kebiche, "Biaxial fatigue analysis model under non-proportional phase loading of tensegrity cable domes," *Eng. Struct.*, vol. 245, p. 112791, 2021, doi: 10.1016/ j.eng struct.2021.112791.

[15] P. Obara, M. Solovei, and J. Tomasik, "Parametric dynamic analysis of tensegrity cable-strut domes," *J. Theor. Appl. Mech.*, vol. 62, no. 2, pp. 253–267, 2024, doi: 10.15632/jtam-pl/183833.

[16] P. Obara, M. Solovei, and J. Tomasik, "Qualitative and quantitative analysis of tensegrity domes," *Bull. Pol. Acad. Sci. Tech. Sci.*, vol. 71, no. 1, p. e144574, 2023, doi: 10.24425/bpasts.2023.144574.

[17] S. Kumar, N. Aswal, and S. Sen, "A novel Genetic algorithm based form-finding approach towards the improved design of tensegrity utility bridge," *Structures*, vol. 58, p. 105401, 2023, doi: 10.1016/j.istruc.2023.105401.

[18] N. Veuve, S. Dalil Safaei, and I.F.C. Smith, "Active control for mid-span connection of a deployable tensegrity footbridge," *Eng. Struct.*, vol. 112, pp. 245–255, 2016.

[19] F. Fraternali, J. de Castro Motta, G. Germano, and E. Babilio, "Mechanical response of tensegrity-origami solar modules," *Appl. Eng. Sci.*, vol. 17, p. 100174, 2024, doi: 10.1016/j.apples.2023.100174.

[20] L. Heping, S. Jian, Q. Yupeng, and L. Ani, "Analysis for a novel folding frame tensegrity tent," *Structures*, vol. 57, p. 105085, 2023, doi: 10.1016/j.istruc.2023.105085.

[21] M.C. Cimmino, R. Miranda, E. Sicignano, A.J.M. Ferreira, R.E. Skelton, and F. Fraternali, "Composite solar facades and wind generators with tensegrity architecture," *Compos. Part B*, vol. 115, pp. 275–281, 2017, doi: 10.1016/j.compositesb.2016.09.077.

[22] M.S. Khaled, M. Chen, E.Z. Losoya, L.A. Rodriguez, E. Gildin, and R.E. Skelton, "Tensegrity laboratory drilling rig for earth and space drilling, mining, and exploration," *Int. J. Solids Struct.*, vol. 252, p. 111785, 2022, doi: 10.1016/j.ijsolstr.2022.111785.

[23] A. Amendola, G. Carpentieri, M. de Oliveira, R.E. Skelton, and F. Fraternali, "Experimental investigation of the softening-stiffening response of a tensegrity prisms under compressive loading," *Compos. Struct.*, vol. 117, pp. 234–243, 2014, doi: 10.1016/j.compstruct.2014.06.022.

[24] F. Fraternali, G. Carpentieri, and A. Amendola, "On the mechanical modeling of the extreme softening/stiffening response of axially loaded tensegrity prisms," *J. Mech. Phys. Solids*, vol. 74, pp. 136–157, 2015, doi: 10.1016/j.jmps.2014.10.010.

[25] Y. Ma *et al.*, "Meta-tensegrity: Design of a tensegrity prism with metal rubber," *Compos. Struct.*, vol. 206, pp. 644–657, 2018, doi: 10.1016/j.compstruct.2018.08.067.

[26] L. Małyszko and A. Rutkiewicz, "Static response of axially loaded tensegrity prism. Example of using proprietary programming language" in *XXII Lightweight Structures in Civil Engineering. Contemporary Problems*. L. Małyszko, Ed., Olsztyn, Poland: University of Warmia and Mazury Press, 2016, pp. 43–48.

[27] I.J. Oppenheim and W.O. Williams, "Geometric Effects in an Elastic Tensegrity Structure," *J. Elast.*, vol. 59, pp. 51–65, 2000.

[28] L. Małyszko and A. Rutkiewicz, "The design of a 3D tensegrity module to EC3 – numerical examples," in *XXVII Lightweight Structures in Civil Engineering. Contemporary Problems*. J. Szafran and M. Kamiński, Eds., Łódź, Poland: Łódź University of Technology Press, 2021, pp. 67–78.

[29] J. Cai, X. Wang, R. Yang, and J. Feng, "Mechanical behavior of tensegrity structures with High-mode imprefections," *Mech. Res. Commun.*, vol. 94, pp. 58–63, 2018, doi: 10.1016/j.mechrescom.2018.09.006.

[30] J. Cai, R. Yang, X. Wang, and J. Feng, "Effect of initial imperfections of struts on the mechanical behavior of tensegrity structures," *Compos. Struct.*, vol. 207, pp. 871–876, 2019, doi: 10.1016/j.compstruct.2018.09.018.

[31] K. Pajunen, P. Johanns, R. Kumar Pal, J.J. Rimoli, and Ch. Daraio, "Design and impact response of a 3D-printable tensegrity-inspired structures," *Mater. Des.*, vol. 182, p. 107966, 2019, doi: 10.1016/j.matdes.2019.107966.

[32] J. Feron, P. Latteur, and L. Rhode-Barbarigos, "Experimental Testing of a Tensegrity Simplex: Self-Stress implementation and Static Loading," *J. Struct. Eng.*, vol. 149, no. 7, p. 04023073, 2023, doi: 10.1061/JSENDH.STENG-11517.

[33] Instron, "Manual M47-16365", 2012.

[34] Bluehill, "Bluehill Manual v.2.6", 2012.

[35] "Autodesk Inventor", Autodesk. [Online]. Available: https://www.autodesk.com/products/inventor.

[36] Eurocode 3: Design of steel structures. Part 1-1: General rules and rules for buildings, 2006.

[37] Z.P. Bazant and L. Cedolin, *Stability of Structures. Elastic, Inelastic, Fracture, and Damage Theories*, New York: Dover Publications, 2003.

[38] MathWorks Inc., "Matlab Programming Fundamentals", Natick, MA, USA, 2020.